Supporting Information

Succinic Anhydride as a Deposition-Regulating Additive for Dendrite-Free Lithium Metal Anodes

Yu-Xiang Xie, [a] Yi-Xin Huang,[a] Xiao-Hong Wu,[a] Chen-Gung Shi,[a] Li-Na Wu,[a] Cun Song,[a] Jing-Jing Fan,[a] Peng Dai,[a] Ling Huang*[a], Ying-Jie Hua,[b] Chong-Tai Wang*[b], Yi-Min Wei,[c] Shi-Gang Sun*[a]

a. State Key Laboratory of Physical Chemistry of Solid Surfaces, Collaborative Innovation Center of Chemistry for Energy Materials, College of Chemistry and Chemical Engineering, Xiamen University, Xiamen, 361005, China
E-mail: huangl@xmu.edu.cn (L. Huang), sgsun@xmu.edu.cn(S. Sun)

b. College of Chemistry and Chemical Engineering, Hainan Normal University, Key Laboratory of Electrochemical Energy Storage and Energy Conversion of Hainan Province, Haikou 571158, China
E-mail: oehy2014@163.com (C. Wang)

c. 21C Innovation Laboratory, Contemporary Amperex Technology Co., Ningde, 352100, China

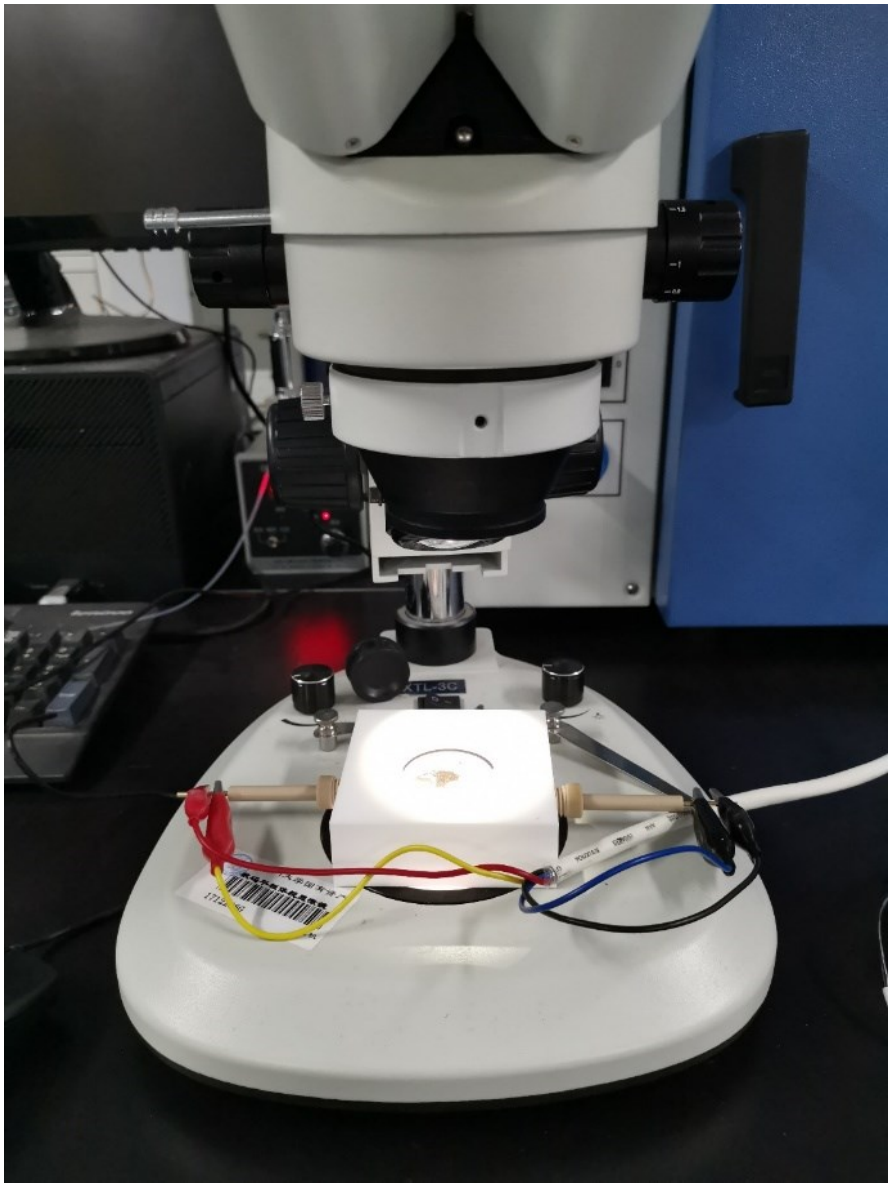

Figure S1. Optical electrochemical cell for in situ optical characterization.

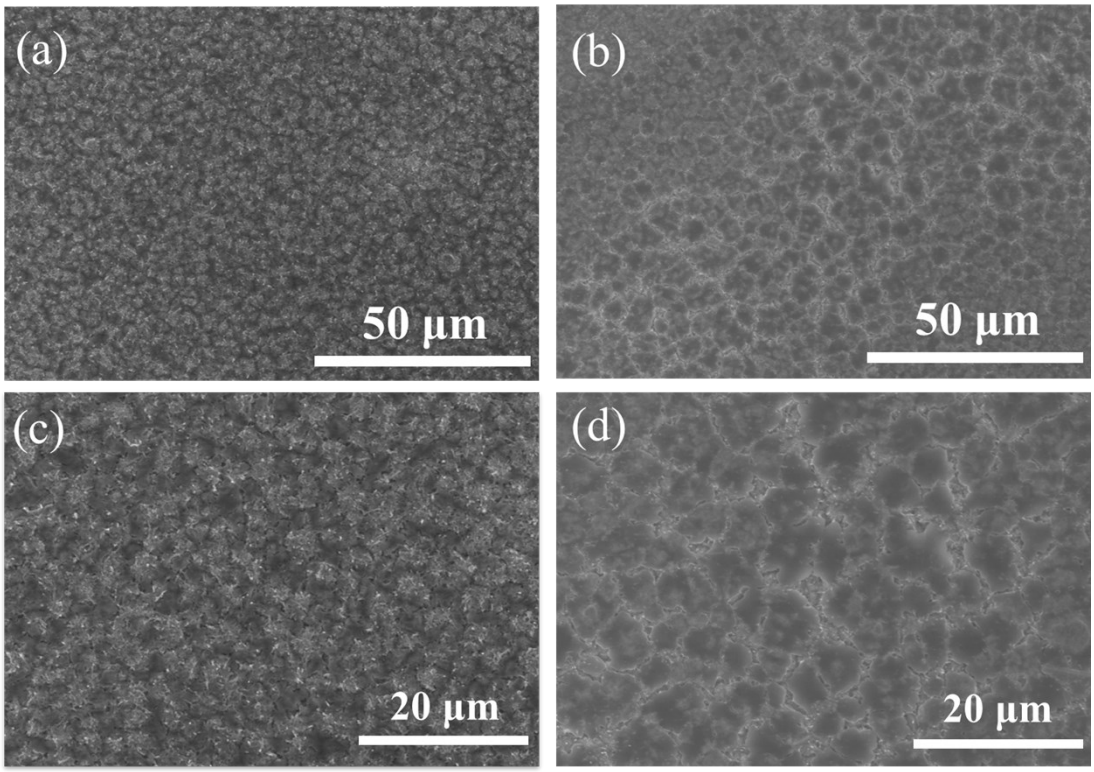

Figure S2. SEM images of Li deposition on a Cu foil without (e) and with 3.0 wt% SA (f) after Li plating for 300 s at a current density of 0.5 mA cm^{-2}.

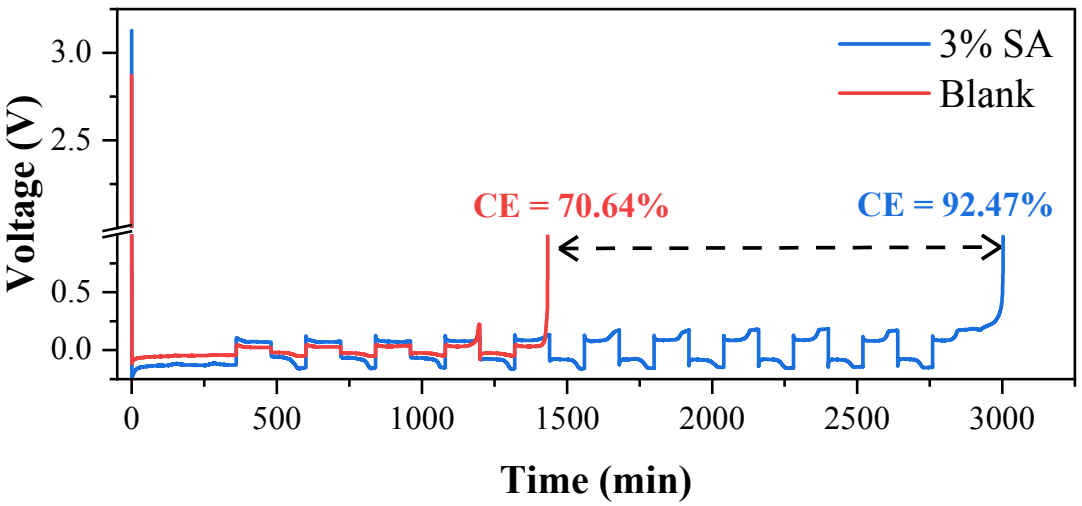

Figure S3. Li plating/stripping CE in Li||Cu cells in electrolytes with and without SA at a current density of 0.5 mA cm^{-2} and a capacity of 1 mAh cm^{-2}.

To simulate the Li plating/stripping cycles of a Li anode and minimize the impact of the Cu substrate, a more accurate coulombic efficiency measurement method was applied here, which is similar to the earlier work.[1] First, a capacity of 3 mAh/cm^2 of Li was deposited on Cu substrate as reversible Li (Qr) at a current of 0.5 mA/cm^2. Then,

one-third of plating Li (1 mAh/cm^2, Q_c) was stripped/plated at same current density each time. Finally, the remaining Li (Q_S) after 10 Li plating/stripping cycles was completely stripped to 1.0 V to calculate the Coulombic efficiency. CE (Coulombic efficiency) can be calculated by the following equation:

$$CE = \frac{10Q_C + Q_s}{10Q_c + Q_r}$$

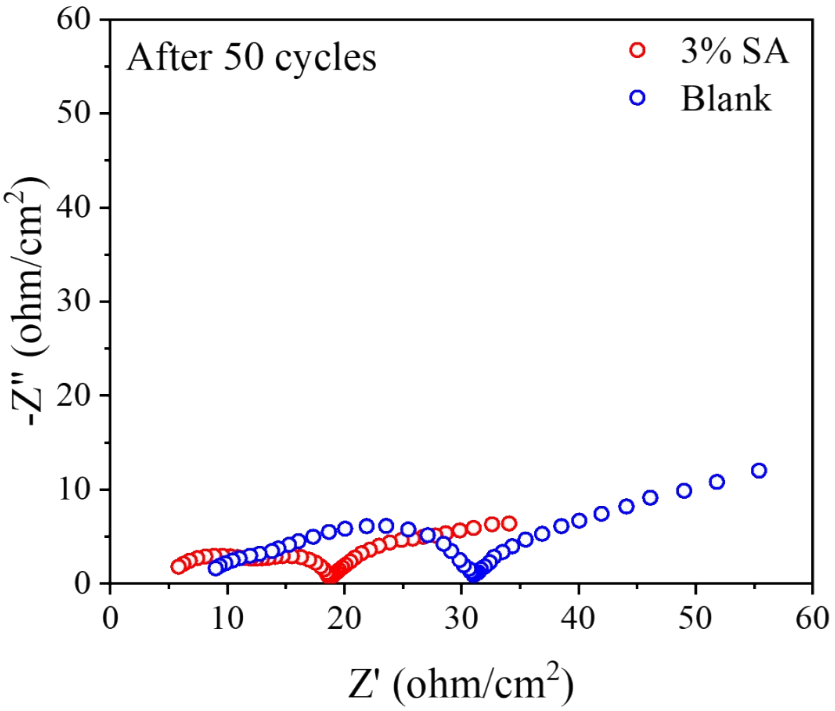

Figure S4. EIS spectra of Li|Li cells after 50 cycles with and without SA as an additive.

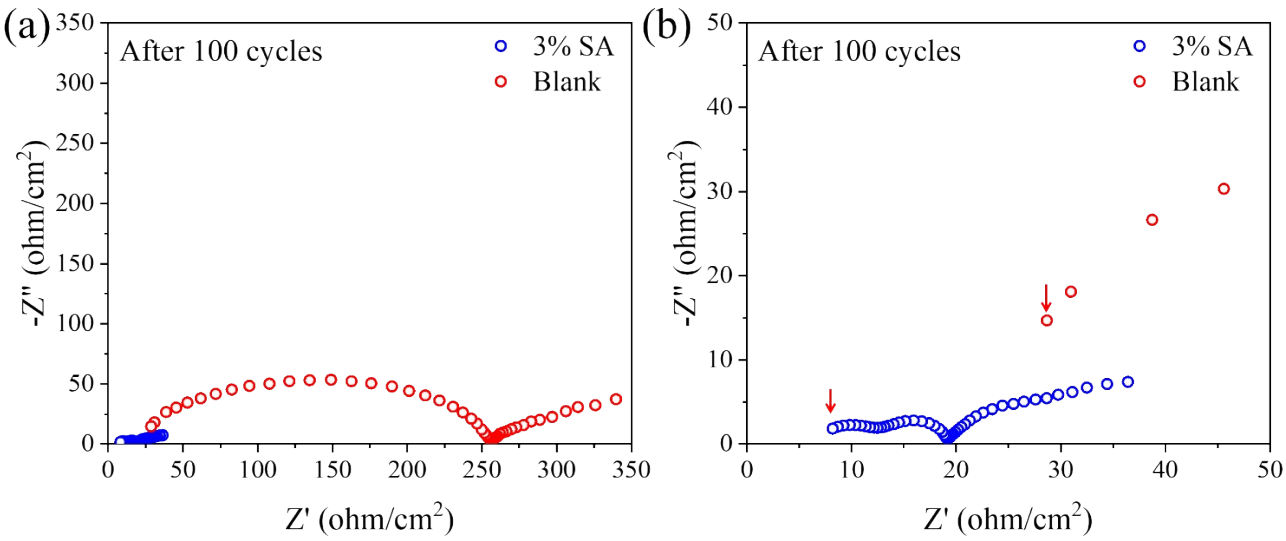

Figure S5. EIS spectra of Li|Li cells after 100 cycles with and without SA as an additive(a), and (b) an enlarged view of the high-frequency region marked by the red rectangle in (a).

Table S1. The comparisons of cycle stability between our work and previous reports

Electrolyte additives	**Current Density (mA cm^{-2})**	**Areal capacity (mAh cm^{-2})**	**Cycle number**	**Years**	**Ref.**
3wt% hexafluoroacetylacetone (HFAA)	1.0	0.5	200	2019	2
3 wt% 15-Crown-5	1.0	0.5	170	2020	3
0.15 M 1,3,5-benzenetrith	0.5	0.5	200	2021	4
1.0 M (Pyr1(12) FSI	0.5	2	~110	2018	5
0.05 M LiPF6 + dual-salt	1.0	0.5	210	2017	6
8 wt% $AlCl_3$	0.5	1.0	~235	2017	7
5% $LiNO_3$	0.5	0.5	150	2019	8
20 mM Boric acid	0.25	0.5	215	2018	9
2 wt% VC + 2 wt% LiDFP	0.5	1.0	200	2020	10
3 wt% SA	1.0	0.5	300	**This work**	**This work**

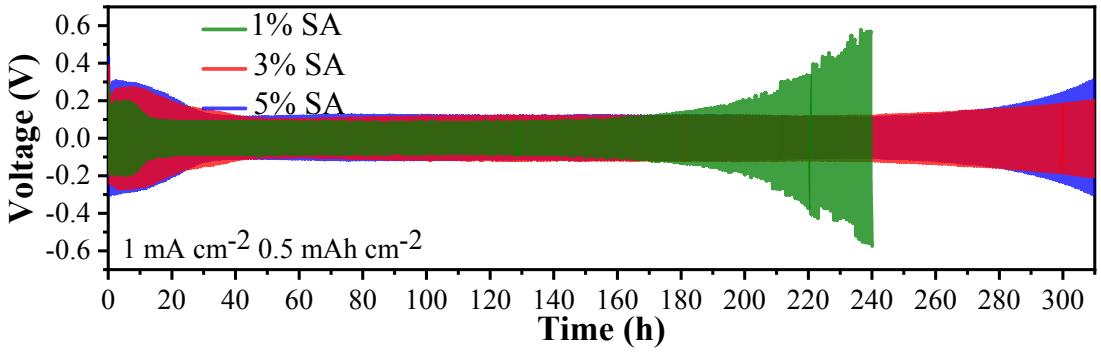

Figure S6. Voltage–time profiles of symmetric cells cycling in 1.0, 3.0, and 5.0 wt% SA-containing electrolytes.

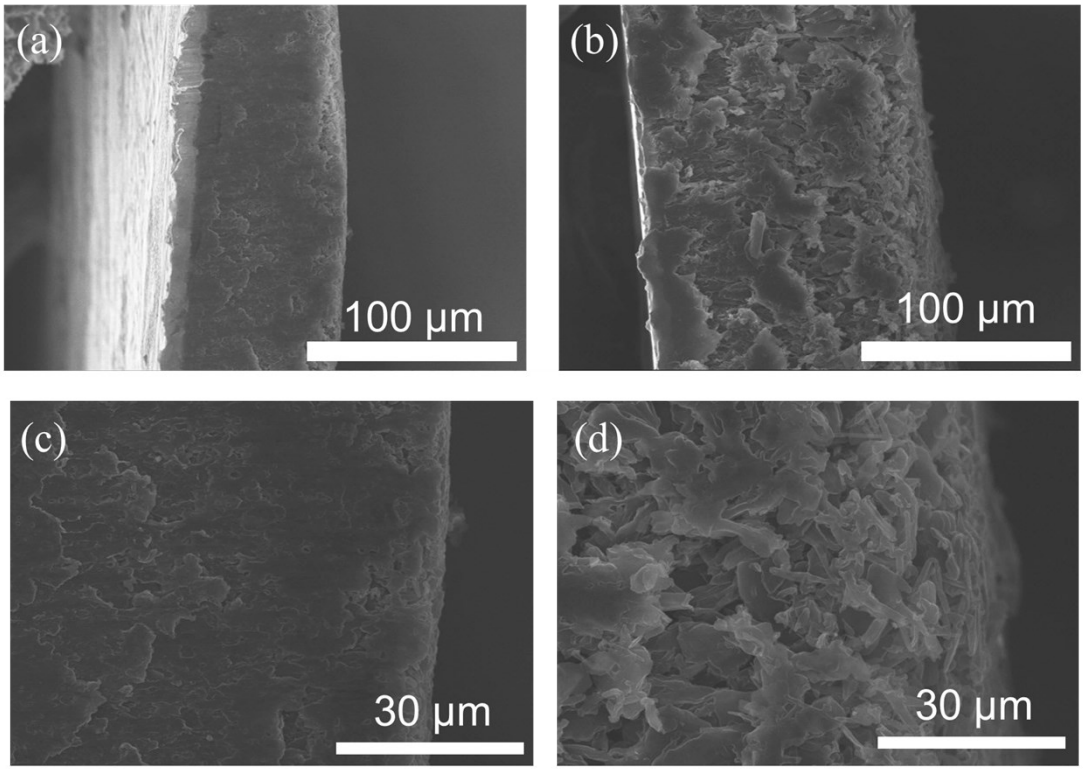

Figure S7. Side-view SEM images of Li deposited (0.5 mA cm^{-2} with a fixed capacity of 8 mAh cm^{-2}) on Cu foil in electrolytes with (a, c) and without (b, d) SA.

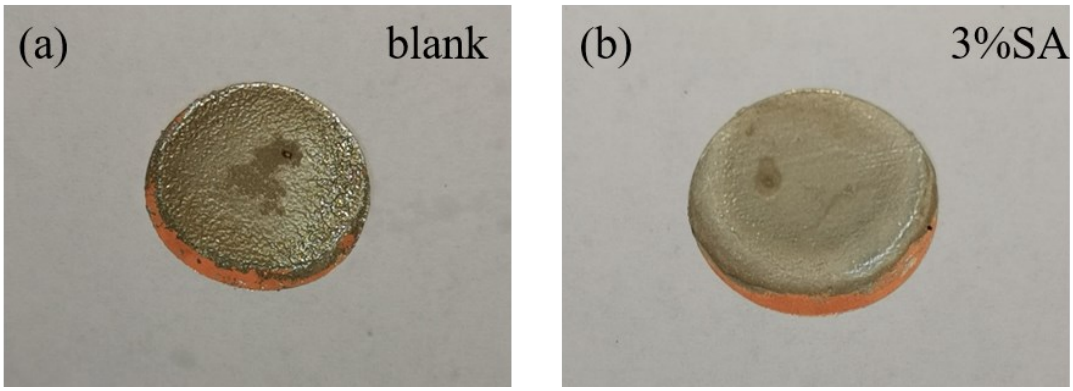

Figure S8. Photographs of Cu substrates after plating at 8 mAh g^{-1} in electrolytes (a) without and (b) with SA.

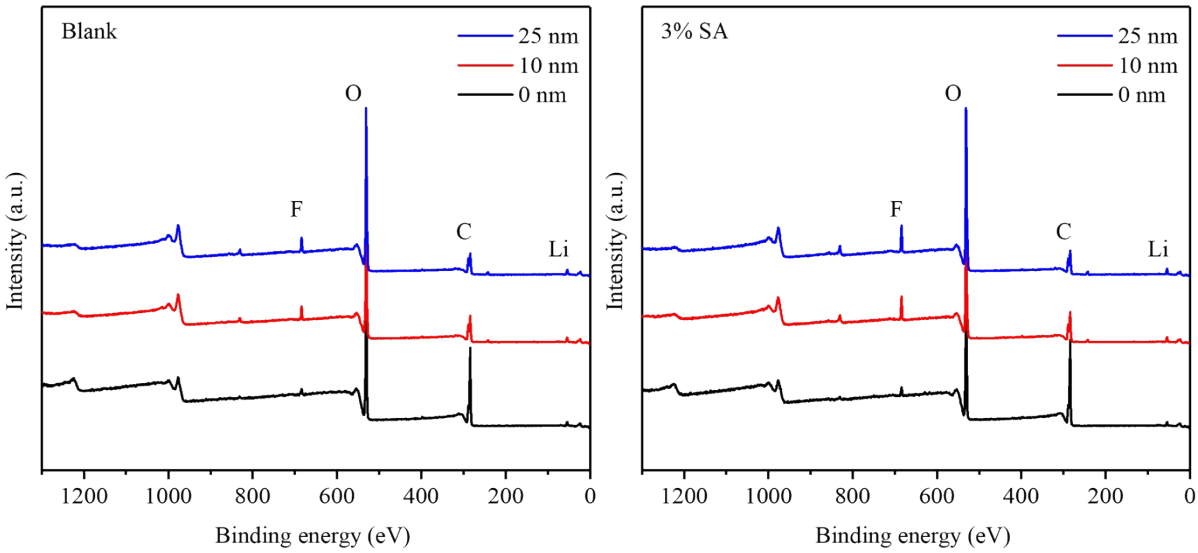

Figure S9. XPS profile of Li|Li cells after 50 cycles with and without SA as an additive.

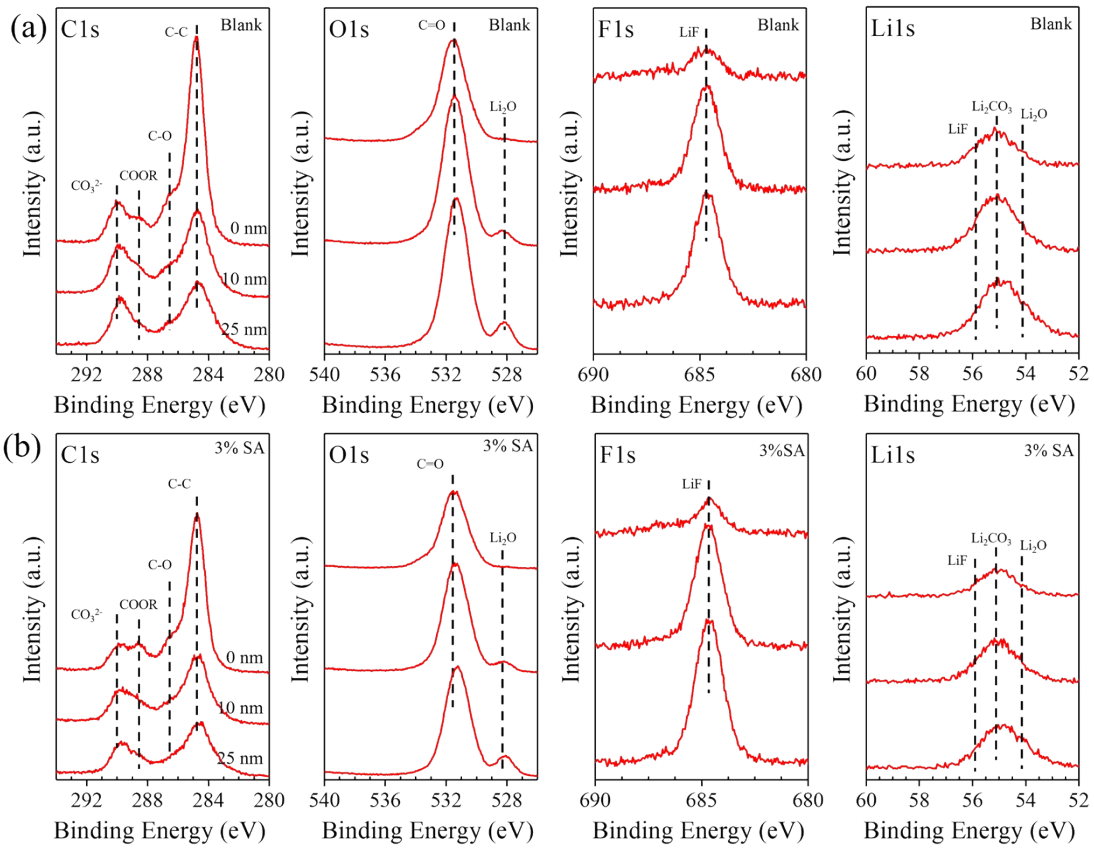

Figure S10. C1s, O1s, F1s, and Li1s XPS profiles of Li|Li cells after 50 cycles with and without SA as an additive.

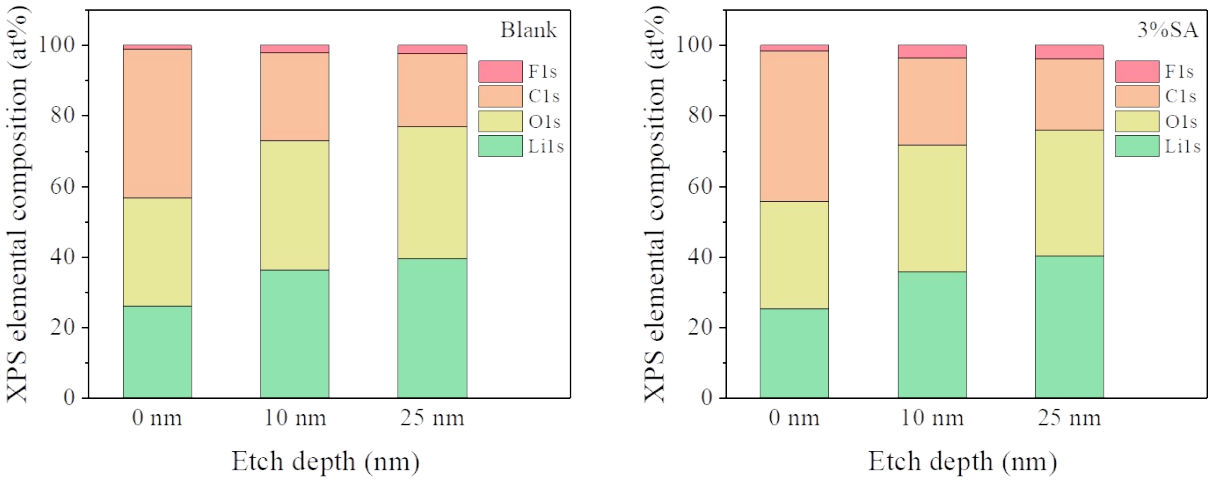

Figure S11. XPS elemental composition of Li|Li cells after 50 cycles in electrolytes with and without SA.

Table S2. XPS elemental compositions of Li|Li cells after 50 cycles without SA as an additive.

XPS elemental composition (at%)				
Etch depth (nm)	Li1s	F1s	C1s	O1s
0	25.9815	**1.0609**	42.181	30.7766
10	36.2092	**2.28529**	24.8257	36.6798
25	39.4103	**2.43315**	20.7525	37.4041

Table S3. XPS elemental compositions of Li|Li cells after 50 cycles with SA as an additive.

XPS elemental composition (at%)				
Etch depth (nm)	Li1s	F1s	C1s	O1s
0	25.3255	**1.56043**	42.75	30.364
10	35.6371	**3.5914**	24.7417	36.0298
25	40.1213	**3.95489**	20.2659	35.6579

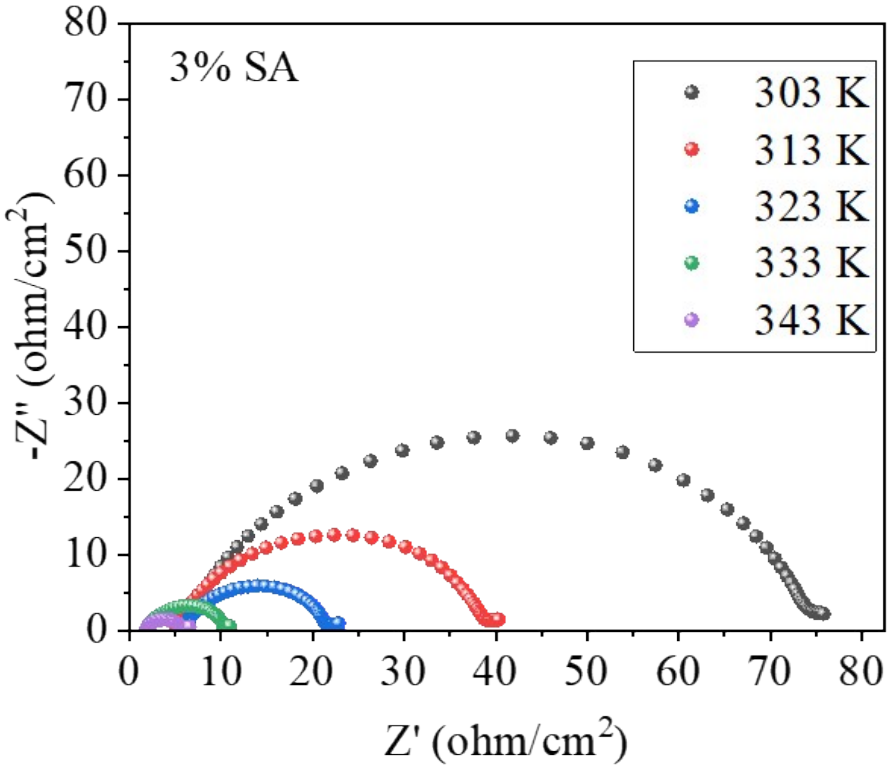

Figure S12. The temperature-dependence of EIS for Li anode formed in electrolyte with 3.0% SA.

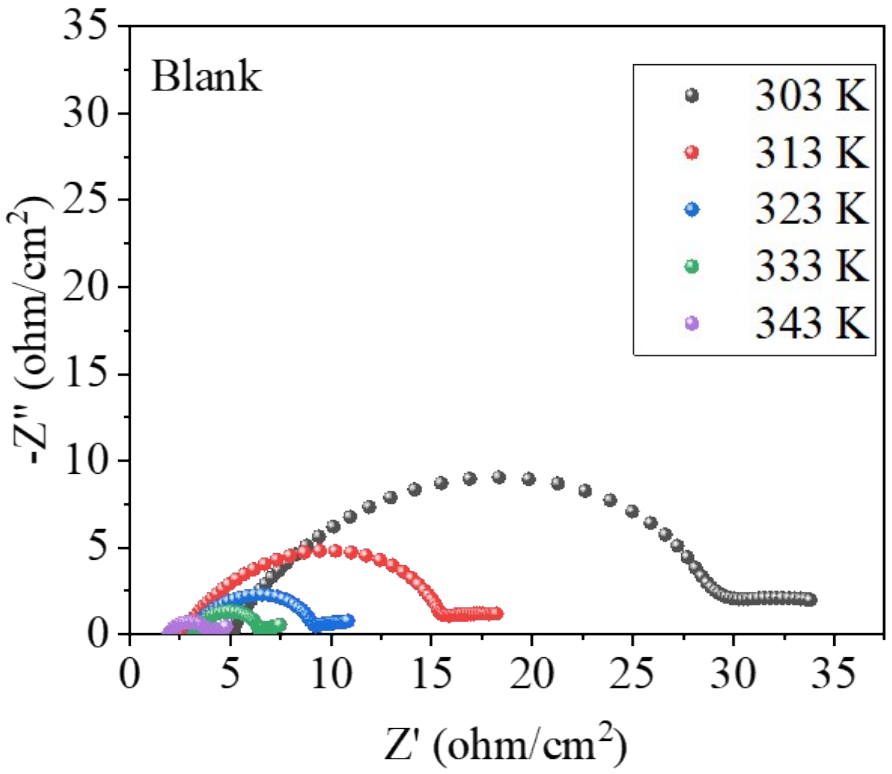

Figure S13. The temperature-dependence of EIS for Li anode formed in electrolyte without SA.

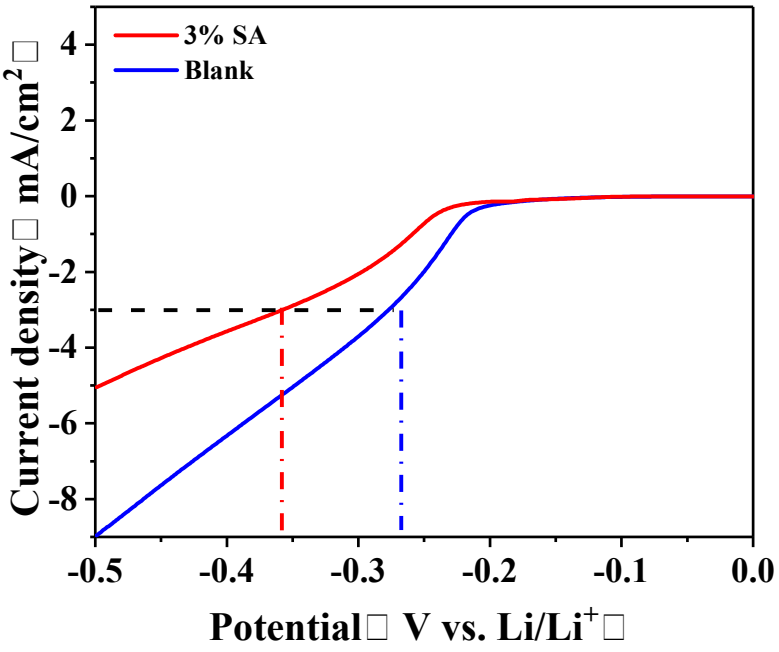

Figure S14. LSV curves of electrolytes with and without SA as an additive.

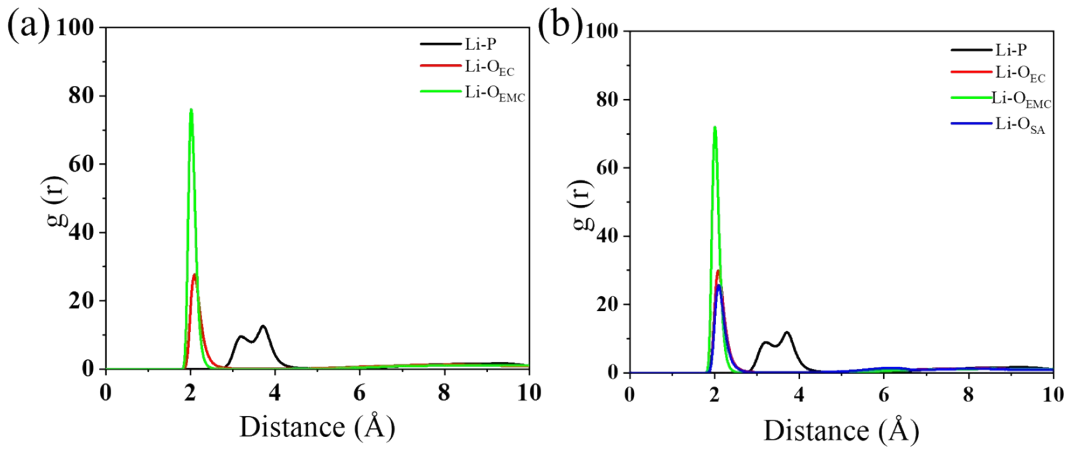

Figure S15. Radial distribution function ($g(r)$) of Li^+ in (a) blank and (b) SA-containing electrolytes.

Supplementary References

1. Adams, B. D.; Zheng, J.; Ren, X.; Xu, W.; Zhang, J.-G., Accurate Determination of Coulombic Efficiency for Lithium Metal Anodes and Lithium Metal Batteries. *Advanced Energy Materials* **2018,** *8* (7), 1702097.
2. Dong, J.; Dai, H.; Fan, Q.; Lai, C.; Zhang, S., Grain refining mechanisms: Initial levelling stage during nucleation for high-stability lithium anodes. *Nano Energy* **2019,** *66*.
3. Wang, H.; He, J.; Liu, J.; Qi, S.; Wu, M.; Wen, J.; Chen, Y.; Feng, Y.; Ma, J., Electrolytes Enriched by Crown Ethers for Lithium Metal Batteries. *Advanced Functional Materials* **2020,** *31* (2).
4. Guo, W.; Zhang, W.; Si, Y.; Wang, D.; Fu, Y.; Manthiram, A., Artificial dual solid-electrolyte interfaces based on in situ organothiol transformation in lithium sulfur battery. *Nat Commun* **2021,** *12* (1), 3031.
5. Yoo, D.-J.; Kim, K. J.; Choi, J. W., The Synergistic Effect of Cation and Anion of an Ionic Liquid Additive for Lithium Metal Anodes. *Advanced Energy Materials* **2018,** *8* (11).
6. Zheng, J.; Engelhard, M. H.; Mei, D.; Jiao, S.; Polzin, B. J.; Zhang, J.-G.; Xu, W., Electrolyte additive enabled fast charging and stable cycling lithium metal batteries. *Nature Energy* **2017,** *2* (3).
7. Ye, H.; Yin, Y.-X.; Zhang, S.-F.; Shi, Y.; Liu, L.; Zeng, X.-X.; Wen, R.; Guo, Y.-G.; Wan, L.-J., Synergism of Al-containing solid electrolyte interphase layer and Al-based colloidal particles for stable lithium anode. *Nano Energy* **2017,** *36*, 411-417.
8. Tan, S. J.; Yue, J.; Hu, X. C.; Shen, Z. Z.; Wang, W. P.; Li, J. Y.; Zuo, T. T.; Duan, H.; Xiao, Y.; Yin, Y. X.; Wen, R.; Guo, Y. G., Nitriding-Interface-Regulated Lithium Plating Enables Flame-Retardant Electrolytes for High-Voltage

Lithium Metal Batteries. *Angew Chem Int Ed Engl* **2019,** *58* (23), 7802-7807.
9. Huang, Z.; Ren, J.; Zhang, W.; Xie, M.; Li, Y.; Sun, D.; Shen, Y.; Huang, Y., Protecting the Li-Metal Anode in a Li-O2 Battery by using Boric Acid as an SEI-Forming Additive. *Adv Mater* **2018,** *30* (39), e1803270.
10. Zheng, G.; Xiang, Y.; Chen, S.; Ganapathy, S.; Verhallen, T. W.; Liu, M.; Zhong, G.; Zhu, J.; Han, X.; Wang, W.; Zhao, W.; Wagemaker, M.; Yang, Y., Additives synergy for stable interface formation on rechargeable lithium metal anodes. *Energy Storage Materials* **2020,** *29*, 377-385.

Author Contributions

Y.-X. Xie, L. Huang, C.-T. Wang and S.-G. Sun conceived the concept and supervised the project. Y.-X. Xie, Y.-X. Huang, X.-H. Wu, C. Song, J.-J. Fan, P. Dai and Yi-Min Wei performed materials synthesis and characterization and data analysis. Y.-X. Xie, Y.-X. Huang, and X.-H. Wu, performed theoretical calculations. Y.-X. Xie, Y.-X. Huang, X.-H. Wu, C.-G. Shi, L.-N. Wu, and C. Song carried out battery preparation and electrochemical measurements. Y.-X. Xie, L. Huang, C.-T. Wang, Y.-J. Hua and S.-G. Sun wrote the manuscript. Y.-X. Xie, L. Huang, C.-T. Wang, Yi-Min Wei, Y.-J. Hua and S.-G. Sun revised the manuscript. All authors were contributing to the discussion of the study.